GEOPHYSICS, VOL. 67, NO. 2 (MARCH-APRIL 2002); P. 618–624, 13 FIGS.
10.1190/1.1468623

Finite-difference modeling of wave propagation in a fluid–solid configuration

Robbert van Vossen*, Johan O. A. Robertsson‡, and Chris H. Chapman**

ABSTRACT

Finite-difference (FD) techniques are widely used to model wave propagation through complex structures. Two main sources of error can be identified: (1) from numerical dispersion and numerical anisotropy and (2) by modeling the response of internal grid boundaries. Conventional discretization criteria to reduce the effects of numerical dispersion and numerical anisotropy have long been established (5-8 gridpoints per wavelength for a fourth-order accurate FD scheme). We analyze the second source of errors, comparing different staggered-grid FD solutions to the Cagniard-de Hoop solution in models with fluid–solid contacts. Our results confirm that it is sufficient to rely on conventional discretization criteria if the fluid–solid interface is aligned with the grid. If accurate modeling of the Scholte wave is required, then a new imaging method we propose should be used to allow for conventional sampling of the wavefield to minimize numerical dispersion. However, for an interface not aligned with the grid (irregular interfaces), a spatial sampling of at least 15 gridpoints per minimum wavelength is required to obtain acceptable results, particularly in seismic seabed applications where Scholte waves may need to be modeled more accurately.

INTRODUCTION

Finite-difference (FD) techniques have been widely used to model a broad range of seismic wave propagation problems. One advantage of FD techniques is their ability to model wave propagation in media with fairly general spatial variation of elastic properties. However, particularly for models with sharp discontinuities, FD schemes are by no means free from accuracy problems (Cunha, 1993; Zahradník et al., 1993). Nevertheless, FD methods have been applied successfully to model problems with sharp discontinuities in the past, e.g., by Dougherty and Stephen (1988) and by Robertsson and Holliger (1997).

Particularly interesting is the accuracy of elastic FD solutions for the wavefield in a fluid–solid configuration. Here, several wavefield components are discontinuous; special attention is required to obtain a good representation of the derivatives of the discontinuous fields. It is important to establish the accuracy of modeling a fluid–solid interface for conventional marine seismics but even moreso in seabed seismics and borehole applications, where Scholte waves are generated. The problem of modeling a fluid–solid boundary condition is addressed in several studies—for instance, by Rodrigues (1993). We attempt to offer a complete characterization and quantification of the problem for commonly used FD schemes.

Discretization of a model leads to two types of errors. The first type is numerical dispersion and numerical anisotropy, caused by the dependency of numerical phase and group velocities on grid spacing and grid orientation. Errors are also introduced by modeling internal grid boundaries. Boundary conditions along an internal interface are only implicitly satisfied, and discretization of a medium results in artificial steps at dipping interfaces.

Several alternative methods to avoid staircase fluid–solid interfaces in a discretized model have been proposed. Fornberg (1988) introduces a curvilinear coordinate system so the grid coincides with a smooth interface. Zhang and Symes (1998) propose an extended FD scheme in the vicinity of internal boundaries for discontinuous terms across the interface. Schoenberg-Muir calculus (Muir et al., 1992) solves the gridding problem by representing a stack of flat elastic layers with a homogeneous anisotropic layer. Each grid cell where different material properties are specified is treated as a stack of layers.

The exact position of an interface can be modeled using boundary integral equation techniques or the finite-element (FE) method. Boundary integral equation techniques are efficient in a medium comprised of relatively homogeneous

Manuscript received by the Editor December 13, 1999; revised manuscript received July 23, 2001.
*Utrecht University, Faculty of Earth Sciences, Budapestlaan 4, 3584 CD Utrecht, The Netherlands. E-mail: vossen@geo.uu.nl.
‡Western Geco, Schlumberger House, Solbraveien 23, 1383 Asker, Norway. E-mail: robertsj@oslo.geco-prakla.slb.com.
**Schlumberger Cambridge Research, High Cross, Madingley Road, Cambridge CB3 0EL, U.K. E-mail: chchapman@slb.com.

Reprinted from Geophysics, 67, 618–624. © 2002 Society of Exploration Geophysicists

layers (Bouchon, 1996). Komatitsch et al. (2000) obtain good results in a fluid–solid configuration using a spectral element approach. A disadvantage of FE methods is that, for many applications, it is computationally more expensive than finite differences. Hybrid modeling techniques, combining ray theory, discrete-wavenumber, FD, and FE methods, reduce the computational cost significantly (Moczo et al., 1997; Robertsson et al., 2000; Robertsson and Chapman, 2000).

We compare 2-D FD solutions with an analytical solution for the wavefield reflected at a flat fluid–solid boundary (de Hoop and van der Hijden, 1983). We choose a configuration where Scholte waves are significant arrivals in the recordings as a critical test. The accuracy of the numerical schemes is investigated for different grid spacings, different angles between the orientation of the grid and the fluid–solid boundary, and for different source–receiver configurations. Special attention is paid to the implementation of the fluid–solid interface in the numerical schemes and the consequences for the numerical results.

FINITE-DIFFERENCE METHOD

An FD scheme requires a numerical approximation to the equations which govern wave motion. Important factors contributing to accuracy of FD modeling are the use of high-order differential operators (Dablain, 1986) and staggered grids (e.g., Virieux, 1986). The high-order operators can be used to minimize the effects of numerical dispersion and numerical anisotropy, whereas the staggered scheme is introduced to obtain more accurate and robust operators.

We limit our discussion on the discretization of the elastic equations to the staggered second-order-accurate in both space and time scheme (Virieux, 1986) and the staggered second-order-accurate in time, fourth-order-accurate in space scheme (Levander, 1988; Robertsson et al., 1994). These modeling schemes are referred to as $O(2,2)$ and $O(2,4)$, respectively.

Discretization

A 2-D Cartesian system with a horizontal axis x and a vertical axis z pointing downward demonstrates the discretization of the isotropic P-SV-wave case. Elastic wave motion is governed by the equation of motion and the elastic constitutive equation. These equations can be written as a first-order hyperbolic system for the unknown components of stress (τ_{xx}, τ_{xz}, τ_{zz}) and particle velocity (v_x, v_z):

$$\frac{\partial v_x}{\partial t} = \rho^{-1}\left(\frac{\partial \tau_{xx}}{\partial x} + \frac{\partial \tau_{xz}}{\partial z}\right), \tag{1}$$

$$\frac{\partial v_z}{\partial t} = \rho^{-1}\left(\frac{\partial \tau_{xz}}{\partial x} + \frac{\partial \tau_{zz}}{\partial z}\right), \tag{2}$$

$$\frac{\partial \tau_{xx}}{\partial t} = (\lambda + 2\mu)\frac{\partial v_x}{\partial x} + \lambda\frac{\partial v_z}{\partial z}, \tag{3}$$

$$\frac{\partial \tau_{zz}}{\partial t} = (\lambda + 2\mu)\frac{\partial v_z}{\partial z} + \lambda\frac{\partial v_x}{\partial x}, \tag{4}$$

and

$$\frac{\partial \tau_{xz}}{\partial t} = \mu\left(\frac{\partial v_x}{\partial z} + \frac{\partial v_z}{\partial x}\right), \tag{5}$$

where ρ is the density and λ and μ are the Lamé parameters. Derivatives are discretized using centered finite differences. The $O(2,2)$ scheme uses two points to estimate spatial derivatives, and the $O(2,4)$ scheme uses a four-point spatial differential operator. The $O(2,2)$ scheme was introduced by Virieux (1986) and the $O(2,4)$ scheme by Levander (1988). To limit the effects of numerical dispersion, the $O(2,2)$ scheme requires sampling 10 to 15 gridpoints per minimum wavelength. The $O(2,4)$ scheme requires less dense sampling: 5–8 gridpoints per minimum wavelength. Cunha (1993) proposes a modified-Virieux-staggered grid. The stress fields [equations (3)–(5)] are substituted into equations (1) and (2) to allow the application of short operators to calculate derivatives of (discontinuous) material properties and long operators for the computation of derivatives of field variables.

When the spatial discretization step is fixed, the time step has to be chosen according to the Courant stability criterion to obtain stable results:

$$\Delta t < \gamma\frac{\Delta x}{v_{max}}, \tag{6}$$

where γ is the so-called Courant number, the parameter which controls stability, and v_{max} is the maximum velocity present in the model. The Courant number for the 2-D $O(2,2)$ scheme is (Virieux, 1986)

$$\gamma = \frac{1}{\sqrt{2}}. \tag{7}$$

For the 2-D $O(2,4)$ scheme (Levander, 1988),

$$\gamma = 0.606. \tag{8}$$

Fluid–solid interface

The physical boundary conditions at the fluid–solid interface require (1) the continuity of the normal component of the particle displacement, (2) the equality of the normal component of the traction in the solid and the opposite of the acoustic pressure in the fluid, and (3) the vanishing of the tangential components of the traction in the solid.

Instead of explicitly satisfying the boundary conditions, effective media parameters are used (Boore, 1972; Schoenberg and Muir, 1989; Zahradník et al., 1993; Graves, 1996). Effective media parameters provide a more accurate representation of the actual parameters by appropriately satisfying the traction continuity across the interface (Zahradník et al., 1993). Effective medium parameters in a staggered grid are (Graves, 1996)

$$\bar{\mu}^{i+1/2,j+1/2} = \left[\frac{1}{4}\left(\frac{1}{\mu^{i,j}} + \frac{1}{\mu^{i+1,j}} + \frac{1}{\mu^{i,j+1}} + \frac{1}{\mu^{i+1,j+1}}\right)\right]^{-1}. \tag{9}$$

The arithmetic average value of densities is

$$\bar{\rho}^{i+1/2,j} = \frac{1}{2}(\rho^{i,j} + \rho^{i+1,j}),$$
$$\bar{\rho}^{i,j+1/2} = \frac{1}{2}(\rho^{i,j} + \rho^{i,j+1}). \tag{10}$$

Harmonic averaging of the shear modulus [equation (9)] ensures that shear stresses vanish across the fluid–solid interface (Figure 1). Continuity conditions are satisfied implicitly.

A dipping interface is represented by a staircase of vertical and horizontal fluid–solid boundary segments in the numerical scheme (Figure 2). The steps of the interface in the discretized medium cause deviations in solutions since boundary conditions are satisfied for components normal and tangential to the interface. Muir et al. (1992) show that staircase interfaces cause diffractions in the modeled waveforms.

METHOD

The model consists of two homogeneous layers. The upper layer is a fluid half-space; the lower half-space is an isotropic solid. The fluid density is 1000 kg/m^3, the fluid velocity is 1500 m/s, the solid density is 2500 kg/m^3, the P-wave velocity is 3500 m/s, and the S-wave velocity is 2000 m/s. Both media have no attenuation. As absorbing boundaries, perfectly matched layers (Berenger, 1994; Chew and Liu, 1996) were applied along all sides of the grid. The source and receivers are located in the fluid, 10 m above the interface. The source is a line explosive pressure pulse which emits a 50-Hz Ricker wavelet.

The FD solutions for the wavefield in this configuration are compared with the solutions obtained with the Cagniard-de Hoop method (de Hoop and van der Hijden, 1983). To quantify the accuracy of the numerical solution, we need to define a suitable measure. The recordings obtained from a numerical simulation $f(l\Delta t)$ are compared with the analytical results $g(l\Delta t)$ using the L2 norm error:

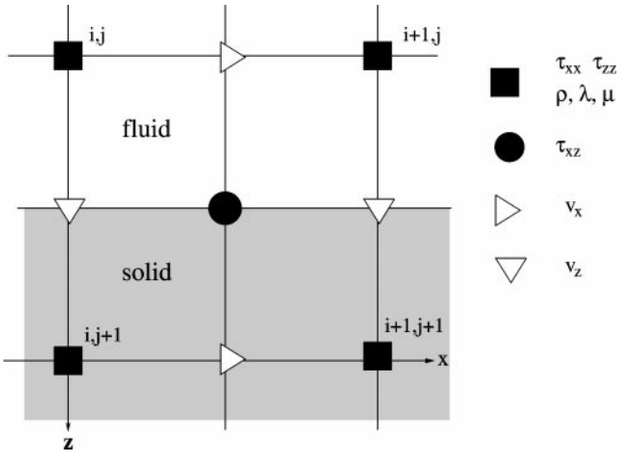

FIG. 1. Fluid–solid interface location for a horizontal flat fluid–solid interface.

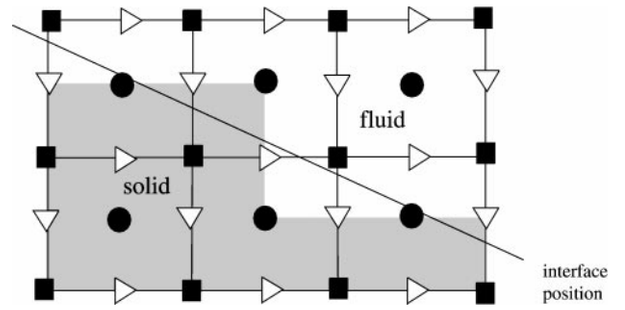

FIG. 2. Implementation of a dipping fluid–solid interface.

$$E = \frac{\sum_{l=0}^{N}(f(l\Delta t) - g(l\Delta t))^2}{\sum_{l=0}^{N} g(l\Delta t)^2}, \qquad (11)$$

where the summation is over all samples of each trace. The direct wave is removed from these records to best analyze the accuracy of the reflected wave, head wave, and Scholte wave. A disadvantage of this error measure is that it is particularly sensitive to time shifts rather than amplitude differences when the waveform is distorted. For this reason, synthetics are also compared directly to the analytical solution.

To compare simulations at different mesh sizes Δx, all simulations are performed at a constant maximum Courant number $\gamma = 0.25$.

Implicit and explicit methods for fluid–solid interface positioning

We investigated at which level in the staggered grid the fluid–solid interface is effectively located. Three analytical solutions for different interface positions—$z = j\Delta z$, $z = (j + 1/2)\Delta z$, and $z = (j + 1)\Delta z$ (see Figure 1)—were compared to the corresponding numerical solution in Figure 3. Interestingly, best results were obtained at the interface position $z = (j + 1)\Delta z$; the interface intersects τ_{xx}, τ_{zz}, and v_x. This is the interface location in the Cagniard-de Hoop solutions.

This result suggests a strategy to satisfy boundary conditions explicitly at the level $z = (j + 1)\Delta z$. By imaging τ_{xz} components as odd functions around the fluid–solid interface, we are assured that τ_{xz} vanishes at this boundary. Robertsson (1996) successfully applies a similar approach for implementing the free-surface condition. Within the fluid, we explicitly set spatial derivatives of shear stresses to zero. Solid material properties are used to compute field variables at the boundary. Effective media parameters are not applied. We refer to this technique as the FD image method.

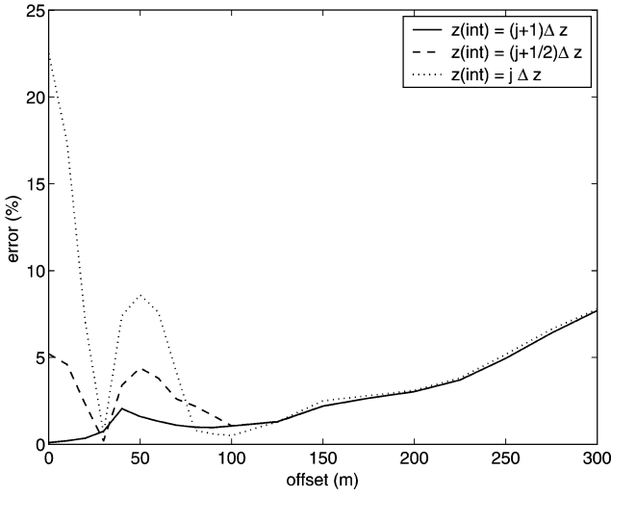

FIG. 3. Comparison between an $O(2,4)$ simulation and analytical results computed for different interface depths $z(int)$. In the FD simulation the uppermost gridpoints with solid material properties are located at $z = (j + 1)\Delta z$. The lowermost gridpoints within the fluid occur at $z = j\Delta z$ (see Figure 1), where $\Delta z = 1.0$ m.

This condition can be applied to smooth interfaces using grid deforming techniques (Fornberg, 1988) so the interface coincides with the grid again. So far, we did not find an accurate method to apply to irregular interfaces.

RESULTS

For synthetic seismograms it is important to establish the relation between desired accuracy and computational cost, i.e., how to discretize the computational domain to obtain acceptable results. Obviously, this depends on the application and the complexity of the model. We investigated three situations: (1) the fluid–solid interface aligned with the grid, (2) the fluid–solid interface not aligned with the grid (in both of these experiments the source and receivers were located near the interface), and (3) an experiment with towed marine survey parameters.

Interface aligned with the grid

Figure 4 displays the error of $O(2,2)$ simulations as a function of offset. The recordings at 500 m offset (Figure 5) consist of the reflected wave and the Scholte wave. The error increases with offset and, as expected, best results are obtained for the finest grid spacings. The numerical result is almost identical to the analytical solution for $\Delta x = 0.5$ m, 30 gridpoints per minimum wavelength. For coarser grid spacings the Scholte wave is delayed and the waveform becomes more and more distorted (numerical dispersion). Effects of numerical dispersion and anisotropy in the $O(2,2)$ solutions are reduced choosing a time step at 80–100% of the limiting Courant number (Alford et al., 1974). However, we chose to work with a relatively low Courant number, $\gamma = 0.25$, to avoid unrealistic high phase and group velocities in the $O(2,4)$ simulations (Levander, 1988). Also, in real full-scale models we often have a lower Courant number at the fluid–solid interface since higher velocities occur elsewhere in the model.

Figure 6 shows the error of $O(2,4)$ simulations as a function of offset. Interestingly, the $O(2,2)$ scheme is overall more accurate than the $O(2,4)$ scheme for a sampling rate up to 15 gridpoints per minimum wavelength ($\Delta x = 1.0$ m). This is caused by the shorter spatial extent of the $O(2,2)$ stencil compared with the $O(2,4)$ scheme. On the other hand the $O(2,4)$ scheme provides more accurate results for coarser grid spacings because of the suppression of numerical dispersion.

Another interesting point is that the $O(2,4)$ Scholte wave propagates faster than the analytical one (Figure 5). Using five gridpoints per minimum wavelength ($\Delta x = 3.0$ m), this effect is counterbalanced by numerical dispersion, which delays and distorts the signal. The L2 error norm is rather sensitive to time shifts, which explains the smaller L2 error of this simulation, but this result actually is worse.

Figure 7 shows the error of $O(2,4)$ image solutions as a function of offset. Now we observe a relatively large error around 50 m offset. From there on, the error decreases with offset. Good results are obtained at large offsets (see Figure 5).

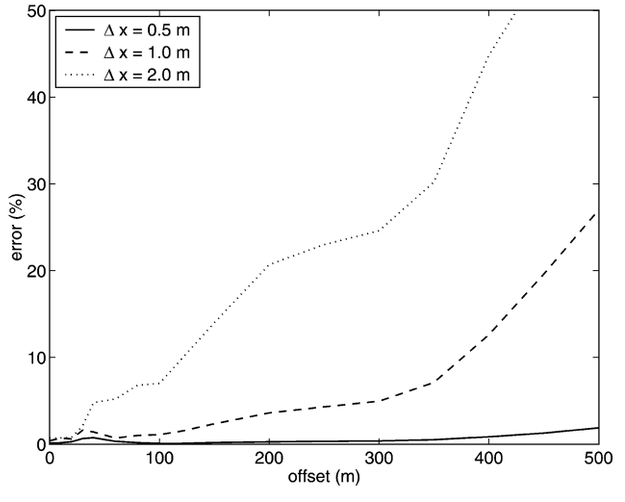

FIG. 4. Relative errors between the $O(2,2)$ scheme and the analytical solution for reflections at a horizontal fluid–solid interface.

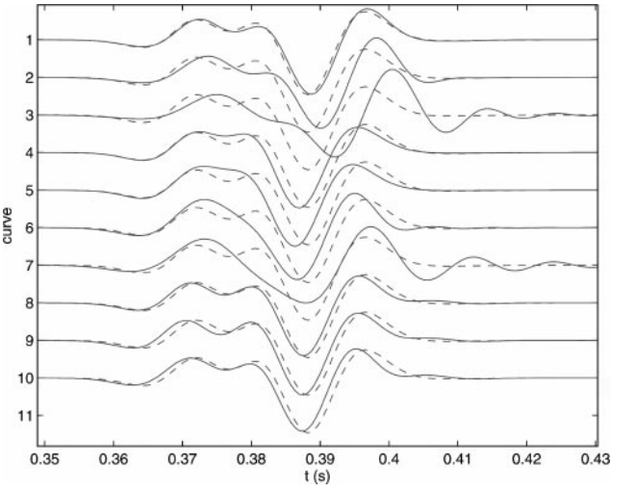

FIG. 5. Comparison of FD solutions with the analytical solution (dashed) at 500 m offset. Curves 1–3 are $O(2,2)$ simulations with $\Delta x = 0.5$, 1.0, and 1.5 m; curves 4–7 are $O(2,4)$ simulations with $\Delta x = 0.5$, 1.0, 2.0, and 3.0 m; and curves 8–10 are $O(2,4)$ image solutions with $\Delta x = 0.5$, 1.0, and 2.0 m, respectively.

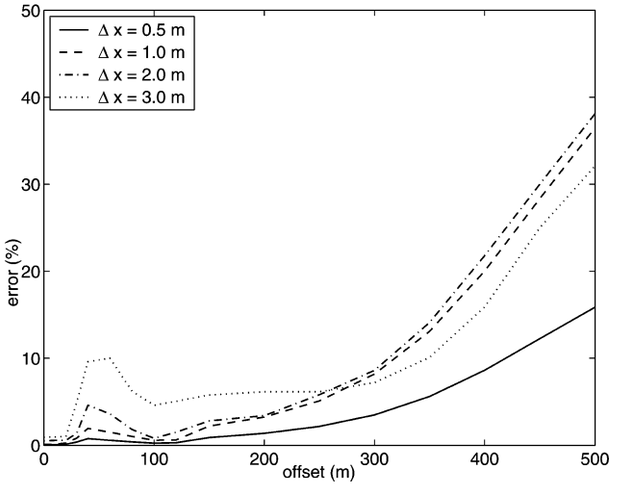

FIG. 6. Relative errors between the $O(2,4)$ scheme and the analytical solution.

In particular, note the small differences between the analytical solution and the numerical solutions for $\Delta x = 0.5$ m and $\Delta x = 2.0$ m, 30 and 7.5 gridpoints per minimum wavelength, respectively. Numerical dispersion is still suppressed, and there is a small time shift between the numerical and analytical solutions. The large error at 50 m offset is caused by a time shift together with destructive interference between the reflected wave and the Scholte wave. A small amplitude results in a larger relative error.

Interface not aligned with the grid

Figures 8–10 show the accuracy of the synthesized wavefield as a function of dipping angle. As expected, best results are obtained when the fluid–solid interface is aligned with the grid (0° and 90°). For dip angles away from 0° and 90°, the error increases and does so more rapidly for coarser grid spacings. Near a dip of 45° the error decreases. This is probably because the interface aligns with gridpoints. Asymmetry between errors at 15° and 75° and between 30° and 60° at zero offset is related to different locations of the steps in the numerical interfaces.

In Figure 11, pressure recordings at 500 m offset are displayed for different dipping angles of the fluid–solid interface. Even for very fine grid spacings there remain substantial differences between numerical and analytical solutions. The error is mainly characterized by a time shift and diffraction in the Scholte wave. The reflected P-wave (the first arrival in the displayed recordings) is modeled accurately.

The error of the $O(2,4)$ simulations is smaller than the error of the $O(2,2)$ simulations (see Figures 11a and b). For an interface not aligned with the grid, the Scholte wave is delayed in the results of both numerical schemes. The time shift of the $O(2,4)$ Scholte waves is smaller; hence, the error is smaller. Moreover, the waveform is less distorted. The second-order scheme is more sensitive to the irregular steps of the interface than the fourth-order scheme is. Recall that for an interface aligned with the grid, the $O(2,2)$ scheme is superior to the $O(2,4)$ scheme when using at least 15 gridpoints per minimum wavelength.

Comparing the two fourth-order simulations, we observe that the error rapidly increases with grid spacing. The Scholte

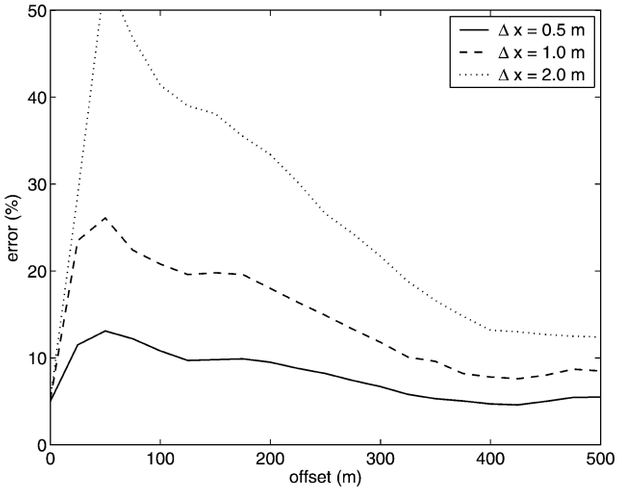

FIG. 7. Relative errors between the $O(2,4)$ image scheme and the analytical solution.

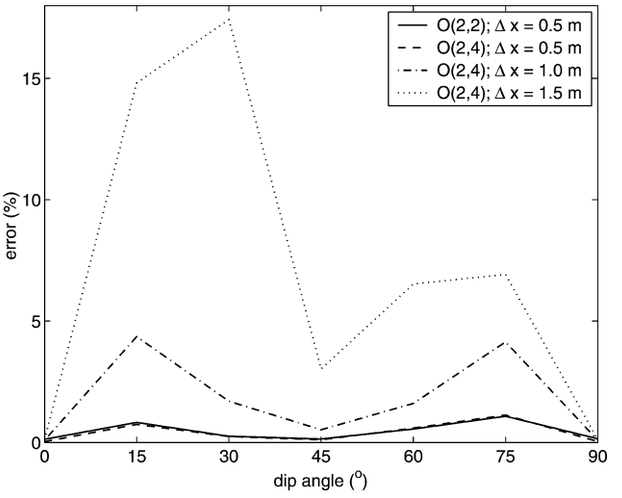

FIG. 8. Error as a function of dipping angle at zero offset for different grid spacings.

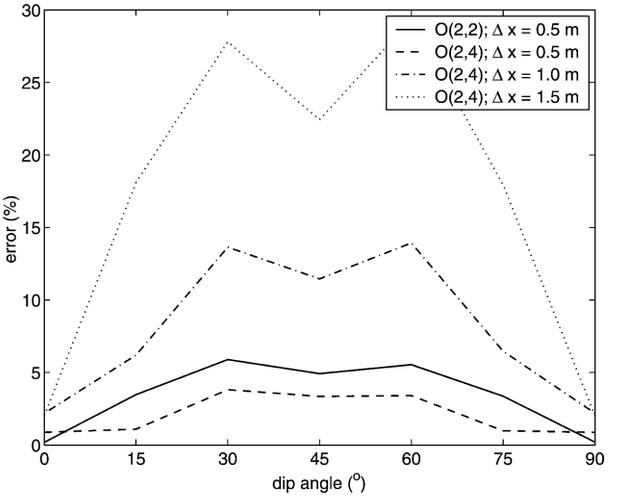

FIG. 9. Error as a function of dipping angle at 150 m offset for different grid spacings.

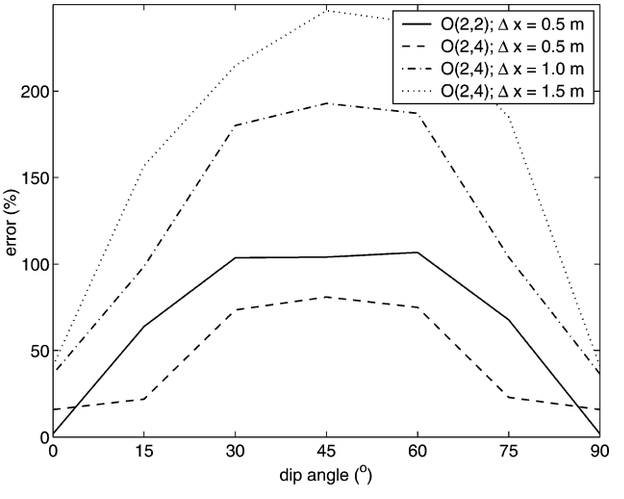

FIG. 10. Error as a function of dipping angle at 500 m offset for different grid spacings.

wave is more delayed and the waveform becomes more distorted. Dense sampling is required to obtain acceptable results.

Towed marine seismic example

So far we have only considered situations where Scholte waves are important arrivals in the recordings. Next we present a simulation to investigate the accuracy of FD simulations using typical towed streamer survey parameters. In this example the model consists of two isotropic half-spaces with no attenuation. The density of the fluid, the upper layer, is 1030 kg/m^3; the density of the solid is 1500 kg/m^3. The fluid velocity is 1460 m/s, whereas the P-wave velocity in the solid is 1700 m/s and the S-wave velocity is 400 m/s. The two layers are separated by a flat interface, dipping 10° with respect to the grid. The source is a line pressure pulse which emanates a 50-Hz Ricker wavelet and is located in the fluid 300 m above the interface. Receivers are located at the same height above the interface. Absorbing boundaries are used on all sides of the model. A free surface is not used since it would make it more difficult to interpret the sea-floor reflection. A section of seismograms from the FD simulation with 0.8 m grid spacing (5 gridpoints per minimum wavelength) is shown in Figure 12, and the error as a function of offset is displayed in Figure 13. Accurate results are obtained at all offsets. In this configuration, interface waves do not contribute to the recordings, and reflected waves are modeled accurately when the effects of numerical dispersion are minimized.

DISCUSSION AND CONCLUSIONS

We have investigated FD modeling of wave propagation in a fluid–solid configuration and compared the results to the Cagniard-de Hoop solution. The results confirm that the FD technique is suitable for computing the wavefield in these models.

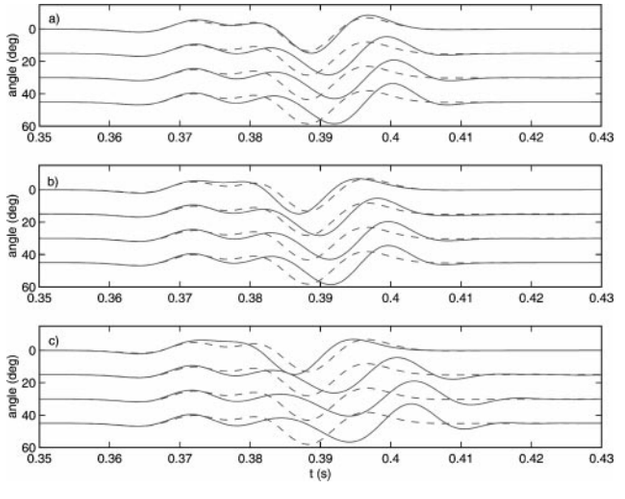

FIG. 11. (a) Pressure recordings at 500 m offset of the $O(2,2)$ scheme ($\Delta x = 0.5$ m) as a function of dipping angle of the fluid–solid interface. The dashed line is the corresponding analytical solution. (b) Pressure recordings at 500 m offset of the $O(2,4)$ scheme, $\Delta x = 0.5$ m. (c) Pressure recordings at 500 m offset of the $O(2,4)$ scheme, $\Delta x = 1.0$ m.

For an interface aligned with the grid, dominant errors are characterized by a time shift in the Scholte wave. The Scholte wave calculated with the $O(2,4)$ scheme has a larger velocity than this wave in the analytical solution, whereas the $O(2,2)$ Scholte wave is delayed. The $O(2,2)$ scheme provides more accurate results than the $O(2,4)$ scheme when using at least a spatial sampling of 15 gridpoints per minimum wavelength. For coarser grid spacings, the $O(2,4)$ scheme is more accurate. The accuracy of the results decreases with offset.

Our image method for the fluid–solid interface provides good results, in particular for coarse grid spacings at larger offsets. In combination with grid deforming techniques (Fornberg, 1988), this could be a very useful method for simulations of seabed seismic surveys.

In the case of dipping interfaces, discretization results in steps in the interface. This causes time delays in the FD solutions compared to the results for a fluid–solid interface aligned with the grid. The main differences between the numerical and

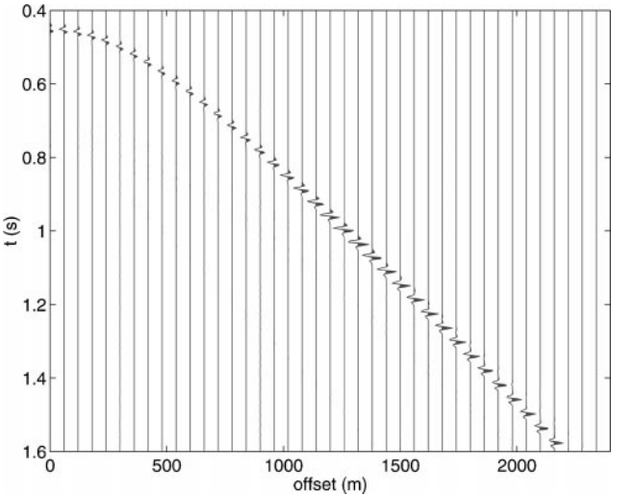

FIG. 12. Part of the seismograms for the towed marine seismic survey example.

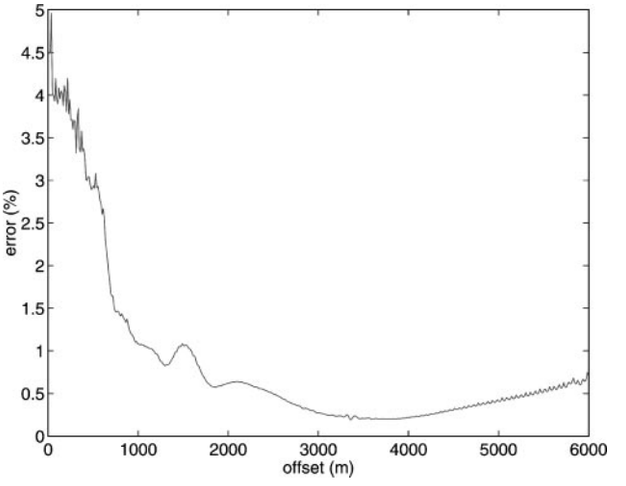

FIG. 13. Error as a function of offset using typical marine towed streamer survey parameters and a 10° dipping interface with respect to the grid.

analytical solutions occur in waves traveling along the interface. For dipping interfaces with respect to the grid, the error rapidly increases with dipping angle until 30°. For dipping interfaces, the $O(2,4)$ scheme is more accurate than the $O(2,2)$ scheme for all grid spacings at all offsets.

A criterion for the number of gridpoints per minimum wavelength is very dependent on the application. Sufficiently accurate results are obtained for towed streamer applications using 5–8 gridpoints per minimum wavelength in the $O(2,4)$ scheme. Here, the Scholte wave does not contribute significantly to the recordings, and the fluid–solid boundary is relatively flat (dipping angle $<10°$). Hence, it is sufficient to rely on the conventional criterion for limiting numerical dispersion in finite differences. In seabed seismic applications, on the other hand, the Scholte wave may need to be modeled more accurately. This requires at least 8–15 gridpoints per minimum wavelength to provide accurate results. Our technique requires a spatial sampling of only 5–8 gridpoints per minimum wavelength to provide good results.

In applications where larger dipping angles of the fluid–solid interface with respect to the grid are expected (e.g., fluid-filled boreholes or sonic tools), larger errors occur in the synthetic data. Reasonably accurate results are obtained using 30 gridpoints per minimum wavelength for all dipping angles. Smaller dipping angles ($<15°$) require a spatial sampling of 15 gridpoints per minimum wavelength.

Similar results are expected in a 3-D fluid–solid configuration.

ACKNOWLEDGMENTS

We thank Roel Snieder, Adrian de Hoop, and Dave Nichols for discussions and helpful suggestions. We also thank Carlos A. Cunha, D. Rodrigues, an anonymous reviewer, and the associate editor for their suggestions when reviewing the paper.

REFERENCES

Alford, R. M., Kelly, K. R., and Boore, D. M., 1974, Accuracy of finite-difference modeling of the acoustic wave equation: Geophysics, **39**, 834–842.

Berenger, J. P., 1994, A perfectly matched layer for the absorption of electromagnetic waves: J. Comput. Phys., **114**, 185–200.

Boore, D. M., 1972, Finite-difference methods for seismic wave propagation in heterogeneous materials, *in* Bolt, B. A., Ed., Methods in computational physics, **11**: Academic Press Inc., 1–37.

Bouchon, M., 1996, The discrete wave number formulation of boundary integral equations and boundary element methods: A review with applications to the simulation of seismic wave propagation in complex geological structures: Pure Appl. Geophys., **148**, 3–20.

Chew, W. C., and Liu, Q. H., 1996, Perfectly matched layers for elastodynamics: A new absorbing boundary condition: J. Comput. Acoust., **4**, 341–359.

Cunha, C. A., 1993, Elastic modeling in discontinuous media: Geophysics, **58**, 1840–1851.

Dablain, M. A., 1986, The application of high-order differencing to the scalar wave equation: Geophysics, **51**, 54–66.

de Hoop, A. T., and van der Hijden, J. H. M. T., 1983, Generation of acoustic waves by an impulsive line source in a fluid/solid configuration with a plane boundary: J. Acoust. Soc. Am., **74**, 333–342.

Dougherty, M. E., and Stephen, R. A., 1988, Seismic energy partitioning and scattering in laterally heterogeneous ocean crust: Pure Appl. Geophys., **128**, 195–229.

Fornberg, B., 1988, The pseudospectral method: Accurate representation of interfaces in elastic wave calculations: Geophysics, **53**, 625–637.

Graves, R. W., 1996, Simulating seismic wave propagation in 3D elastic media using staggered-grid finite differences: Bull. Seis. Soc. Am., **86**, 1091–1106.

Komatitsch, D., Barnes, C., and Tromp, J., 2000, Wave propagation near a fluid–solid interface: A spectral element approach: Geophysics, **65**, 623–631.

Levander, A. R., 1988, Fourth-order finite-difference P-SV seismograms: Geophysics, **53**, 1425–1435.

Moczo, P., Bystrický, E., Kristek, J., Carcione, J. M., and Bouchon, M., 1997, Hybrid modeling of P-SV seismic motion at inhomogeneous viscoelastic topographic structures: Bull. Seis. Soc. Am., **87**, 1305–1323.

Muir, F., Dellinger, J., Etgen, J., and Nichols, D., 1992, Modeling elastic fields across irregular boundaries: Geophysics, **57**, 1189–1193.

Robertsson, J. O. A., 1996, A numerical free-surface condition for elastic/viscoelastic finite-difference modeling in the presence of topography: Geophysics, **61**, 1921–1934.

Robertsson, J. O. A., and Chapman, C. H., 2000, An efficient method for calculating finite-difference seismograms after model alterations: Geophysics, **65**, 907–918.

Robertsson, J. O. A., and Holliger, K., 1997, Modeling of seismic wave propagation near the earth's surface: Phys. Earth Plan. Int., **104**, 193–211.

Robertsson, J. O. A., Blanch, J. O., and Symes, W. W., 1994, Viscoelastic finite-difference modeling: Geophysics, **59**, 1444–1456.

Robertsson, J. O. A., Ryan-Grigor, S., Sayers, C. M., and Chapman, C. H., 2000, A finite-difference injection approach to modeling seismic fluid flow monitoring: Geophysics, **65**, 896–906.

Rodrigues, D., 1993, Large scale modeling of seismic wave propagation: Ph.D. thesis, École Centrale Paris.

Schoenberg, M., and Muir, F., 1989, A calculus for finely layered anisotropic media: Geophysics, **54**, 581–589.

Virieux, J., 1986, P-SV wave propagation in heterogeneous media: Velocity-stress finite-difference method: Geophysics, **51**, 889–899.

Zahradník, J., Moczo, P., and Hron, F., 1993, Testing four elastic finite-difference schemes for behaviour at discontinuities: Bull. Seis. Soc. Am., **83**, 107–129.

Zhang, C., and Symes, W. W., 1998, Fourth order methods for acoustic waves with discontinuous materials, *in* DeSanto, J. A., Ed., Mathematical and numerical aspects of wave propagation: Soc. Ind. Appl. Math., 652–656.